Transactions of the Materials Research Society of Japan. Vol. 20

Optical Absorption and ESR Characterization of $CuInSe_2$ and Related Compounds

K. Sato

Faculty of Technology, Tokyo University of Agriculture and Technology,
Koganei, Tokyo 184, Japan

Optical absorption and ESR measurements were performed in as-grown and heat-treated bulk single crystals of chalcopyrite semiconductors including $CuInSe_2$. Various parameters relating to transport properties of these materials were obtained from analyses of optical absorption spectra. Change of optical spectra by annealing was discussed in terms of Fermi level motion due to incorporation of intrinsic defects caused by annealing.

1. INTRODUCTION

$CuInSe_2$ and related chalcopyrite compounds have been intensively studied as promising candidates for polycrystalline thin film solar cells materials.[1] These chalcopyrite type semiconductors attract attention because of their versatile optical and electrical properties which can, in principle, be tuned for the specific needs of a particular device structure. In order to realize the tuning of the characteristics of $CuInSe_2$ it is vital to know the dependence of the electrooptical properties of this material on the Fermi level relative to the band edges, since the position of the Fermi level determines the physical properties of semiconductors, *i.e.*, the conductivity type and carrier concentrations, as well as the charged states of deep centers, including those formed by intrinsic defects,[2] and residual transition atom ions. [3]

In this study we report the results of optical absorption and electron spin resonance (ESR) investigations of Cu-III-VI_2 single crystals in connection with the annealing-induced motion of the Fermi level relative to the band edges of respective ternary compounds.

2. OPTICAL ABSORPTION

2.1 Optical absorption of transition metal ions

Transition metal ions doped in semiconductors introduce characteristic optical absorption depending on their valence states as well as the lattice sites which they occupy, leading to specific coloration of crystals due to charge-transfer and crystal field transitions. For this study wide gap I-III-VI_2 such as $CuGaS_2$ and $CuAlS_2$ crystals are suited since they can accommodate most of the electronic states within their band gap. Absorption spectra caused by a series of transition metal impurities in $CuAlS_2$ were summarized in ref. 4, in which charge transfer and crystal field transition are reported.[4]

It was also found that thermal treatments in different atmosphere lead to changes in coloration, which has been explained by the shift of the Fermi level accross the demarcation levels discriminating the valence states, *i.e.*, (+/2+) or (+2/+3) of transition metal impurities. As a typical example, demarcation levels of major residual impurities (Fe, Cr and Ni) in $CuAlS_2$ determined from optical absorption and ESR experiments are illustrated in Fig. 1.[5]

In $CuInSe_2$ and $CuInS_2$, however, due to narrowness of their band gaps, absorption bands due to the crystal field transition in the transition metal ions can only be observed in limited cases where optical transitions occur in the infrared region.[6, 7]

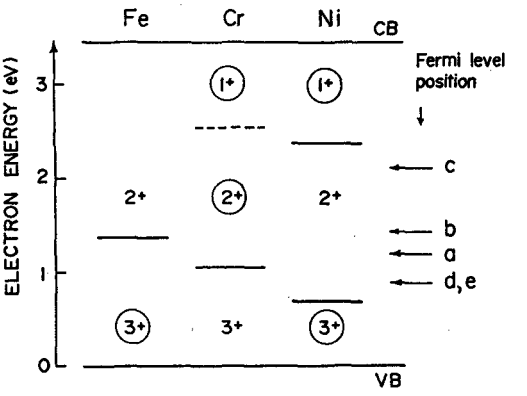

Fig. 1 A schematic energy-level diagram of $CuAlS_2$: Fe, Cr, Ni.The charged states marked by ○ represent those detected by ESR. Demarcation levels (solid horizontal lines) of (2+/3+) in Fe, Cr and Ni as well as that of (+/2+) in Ni are determined by optical absorption. The estimated position of Fermi level in the band gap is indicated in the right part of the figure for; a: as-grown, b: vacuum-annealed, c: Cu-annealed and d and e: S-annealed samples.

2.2 Free carrier absorption

Infrared (IR) absorption spectra in as-grown and heat-treated melt-grown single crystals of $CuInSe_2$ were measured using an FTIR spectrophotometer. The specimens used were as-grown (p-type, ~10^{-1} Ωcm) , vacuum-annealed (n-type, ~1 Ωcm), Cu-annealed (p-type, 10^3 Ωcm) and Se-annealed (p-type, 10^{-1} Ωcm) single crystals. Measurements by means of the van der Pauw technique resulted in the electron mobility of 380 and hole mobility of 26 $cm^2V^{-1}s^{-1}$.

The typical IR spectra of those crystals are shown in Fig. 2.[8] The sharp rise of absorption at the low-energy side of the spectra can be attributed to the free-carrier absorption, which is known to be observable in semiconductors at sufficiently high carrier concentrations.[9] Indeed, we could not observe this absorption in the semi-insulating samples (Cu-annealed) due to the low concentration of free carriers in those samples.

To analyze free carrier absorption we can use classical Drude type formulation,

$$\alpha = \frac{\omega_p^{\,2}\tau}{n_0 c \varepsilon_0} \frac{1}{(\omega\tau)^j + 1}, \qquad (1)$$

where n_0 is the index of refraction, the carrier relaxation time, j the fitting parameter, ω_p the plasma frequency given by $\omega_p=(n_i e^2/m_i\varepsilon_0)^{1/2}$ with n_i and m_i being the concentration and effective mass of electrons (i=e) and holes (i=h). The free carrier concentration n_i can be estimated from the following optical analyses.

In addition to the free carrier absorption, as-grown samples exhibit a broad absorption peak (A-band) at about 3000 cm^{-1} (0.36 eV), which was found to be quenched by annealing in vacuum or in the presence of Cu. Annealing in Se-vapor, on the other hand, resulted in an enhancement of the A-band, as well as in an appearance of a new absorption peak (B-band) at 1200 cm^{-1} (0.14 eV). Such absorption peaks were not observed in n-type crystals, suggesting that these absorption peaks are related with optical transitions between the subbands of the valence band.

For the vacuum-annealed n-type crystals we observed so-called Burstein-Moss shift of the absorption edge amounting to as large as 10 meV, suggesting that the samples are degenerate. The Fermi level position was then located at 109 meV above the bottom of the conduction band taking into account the ratio of effective masses of electrons and holes. (For details refer to our previous paper.[8]) Electron concentration was estimated by the following formula,

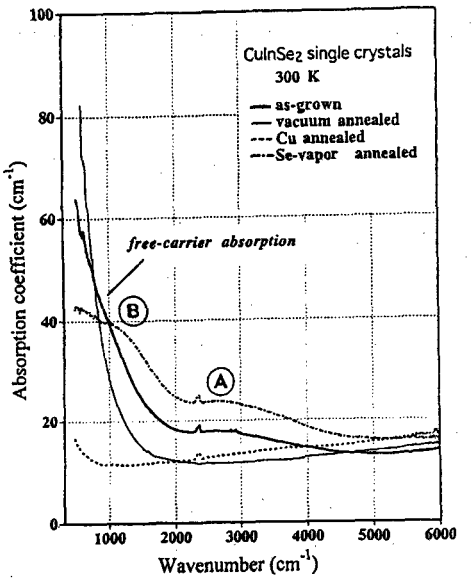

Fig. 2 IR absorption spectra of the $CuInSe_2$ crystals: as-grown (———), vacuum-annealed (——), Cu-annealed (· · · ·), and Se-annealed (— · —).

$$n_c = 4\pi\left(\frac{2m_e}{\hbar^2}\right)^{\frac{3}{2}} \int_{E_c} \frac{E^{\frac{1}{2}}}{1+\exp\left(\frac{E-E_f}{k_BT}\right)} dE, \qquad (2)$$

to be n_c~7×10^{18} cm^{-3}. This value is in good agreement with the value of n_c~3.5×10^{18} cm^{-3} determined by the Hall measurement. Using the eq. (1) and applying the value of n_c thus obtained we calculated free electron spectrum that provides the best fit to the experimental curve, from which j_e and τ_e were determined as 2.14 and 3.7×10^{-14} s, respectively. Electron mobility estimated by using

$$\mu_e = \frac{e\tau_e}{m_e} \qquad (3)$$

was 733 $cm^2V^{-1}s^{-1}$. This value is comparable to the value of 380 $cm^2V^{-1}s^{-1}$ determined by Hall measurements in Cu-annealed n-type crystal.

On the other hand, the hole concentration in as-grown p-type crystals were estimated by the following procedure. From the onset energy position of the A-absorption, energy position of the lowest unfilled level in the valence band E_{hp} was calculated using

$$E_A \approx \Delta_{so} + E_{hp}\left(\frac{m_{hh}}{m_{sh}} - 1\right) \qquad (4)$$

where Δ_{so} is spin-orbit splitting between the heavy hole band and the split-off hole band, and m_{hh} and m_{sh} are effective masses of the heavy hole and split-off hole, respectively. The position of E_{hp} thus

calculated was 16 meV below the top of the valence band. Fermi level position in this case was estimated as being at 84 meV above the top of the valence band at room temperature. Since we know the Fermi-level position, the concentration of holes in as-grown p-type crystal can be estimated by Boltzmann distribution function

$$n_h = 2\left(\frac{2\pi m_h k_B T}{\hbar^2}\right)^{\frac{3}{2}} \exp\left(\frac{E_v - E_f}{k_B T}\right). \quad (5)$$

The room temperature concentration of holes thus calculated was 5.6×10^{17} cm^{-3}. The free carrier absorption spectrum in as-grown p-type crystal was fitted using eq.(1) with the hole concentration obtained above. The fitting parameters were determined as j_h=2.02 and τ_h=1.3×10^{-14} s, from which hole mobility of μ_h=31 $cm^2V^{-1}s^{-1}$ was obtained. This is also in considerably good agreement with the value of 26 $cm^2V^{-1}s^{-1}$ obtained by Hall measurements.

We have thus demonstrated that nondestructive contact-free characterization of transport properties is possible in $CuInSe_2$ only by optical method.

3. CHARACTERIZATION BY ESR

3.1 ESR spectra of Fe^{3+} in Cu-III-VI_2 crystals

Fe is the most easily detected residual impurity species in any of Cu-III-VI_2 crystals by conventional ESR technique. Even in melt-grown crystals in which concentration of Fe impurity is less than the detection limit of EPMA analysis, ESR can clearly detect the trace of the impurity in these materials.

Fe^{3+}-related ESR spectra in a series of as-grown p-type crystals are shown in Figs 3(a) and 3(b) for sulfides and selenides, respectively. The ESR spectra for the Fe^{3+} impurity in all sulfides studied (Fig. 3(a)) exhibit a well-known 5-line fine structure transitions of an ion with $3d^5$-configuration, occupying lattice sites of the tetragonal symmetry. The spin Hamiltonian contains the terms corresponding to the cubic and axial components of the crystal field.[10]

To the contrary, the Fe^{3+}-originated signal of selenides (Fig. 3(b)) exhibits several anisotropic lines with g ~ 2 - 6 together with a nearly isotropic line at g ~ 4.3, resulting from transitions within three Kramers doublets split from the sixfold-degenerate $^6S_{5/2}$ ground state of Fe^{3+} due to the effect of a strong noncubic crystal field containing both axial and rhombic components.[11] The Hamiltonian of the Fe^{3+} ion in the non-cubic crystal field reads,

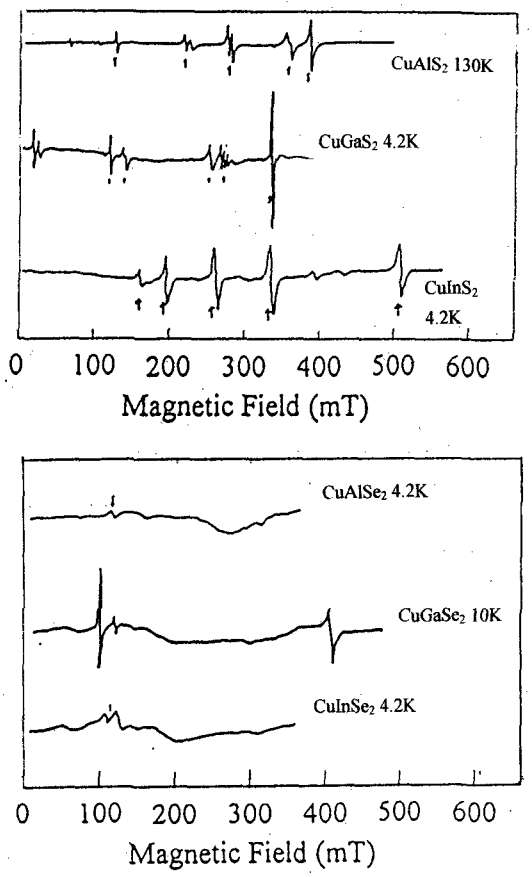

Fig. 3 Fe^{3+}-related ESR signals in Cu-III-VI_2 single crystals: (a) sulfides, (b) selenides.

$$H = g\beta\vec{H}S + D\left(S_z^2 - \frac{1}{3}S(S+1)\right) + E\left(S_x^2 - S_y^2\right), \quad (6)$$

where D and E are parameters of the axial and rhombic components of the crystal field, respectively.

The solutions of the above Hamiltonian depend on the parameter $\lambda = E/D$, describing the relative strength of the axial and rhombic terms of the crystal field. If $E \gg D$, we should observe a nearly isotropic signal near $g = 4.3$, which is in accordance with our results. For the second limiting case, when $E \ll D$, we may expect an anisotropic signal consisting of several lines with g-values in the range 2 – 6, which has also been detected in our $CuInSe_2$ crystals.

3.2 ESR spectra of Fe^{2+} in Cu-III-VI_2 crystals

In vacuum-annealed n-type crystals of $CuInSe_2$ considerably anisotropic signal as shown by II signal with the peak-to-peak line width ΔH_{pp} = 4 mT and effective g-value of $g_{eff//}$=28.7. Such anisotropic ESR signal was commonly observed in many of Cu-III-VI_2 crystals. The

effective g-factor takes its maximum value of $g_{eff//}$=9.5 in $CuAlS_2$ and $g_{eff//}$=14.5 in $CuInS_2$ when the tetragonal c-axis of the crystal is parallel to the external magnetic field ($g_{eff\perp}$~0 for this signal).

Such anisotropic signal has been attributed to the substitutional divalent iron impurity, the signal originating from the magnetically allowed microwave transitions +2⇔-2 within the lowest Ms=± 2 non-Kramers doublet in Fe^{2+}.[12]

3.3 Effect of annealing

Figure 4 shows how ESR spectrum varies with the atmosphere in which crystals are annealed. The observed changes in the ESR spectra of the $CuInSe_2$ crystals, caused by thermal treatments in various atmospheres, can be explained by the annealing-induced motion of the Fermi level relative to the energy band edges.

The Fermi level in the as-grown p-type crystals was situated only 80 meV above the top of the valence band from the IR absorption measurements and, hence, should be below the Fe^{2+}/Fe^{3+} demarcation level, the latter having been located in the midst of the band gap. Therefore, we could observe only the Fe^{3+}-related signal I in the ESR spectra of the as-grown samples.

Annealing in vacuum leads to the change of the conductivity type, wherein the samples are converted into the degenerate n-type ones. This indicates that the Fermi level is shifted upwards and is positioned inside the conduction band far above the Fe^{2+}/Fe^{3+} demarcation level, which in turn leads to a quenching of Fe^{3+} signal I and an appearance of Fe^{2+} signal II. On the other hand, Cu-annealing locates the Fermi level in the midst of the band gap close to the Fe^{2+}/Fe^{3+} demarcation level. Therefore, we can expect both signal I and signal II at room temperature. Annealing in vacuum also results in a drastic increase in the concentration of the V_{Cu}-defects, which leads to an appearance of the signals III from carriers trapped by the defect.

Annealing in the Se-vapor results in a reverse process, wherein the Fermi level is shifted down towards the valence band (and below the Fe^{2+}/Fe^{3+} demarcation level), which results in the highly conductive p-type nature.

4. CONCLUSION.

From the studies introduced above, it has been clarified that optical absorption and ESR measurements provide important information on the parameters of carrier transport as well as that on the position of Fermi level in Cu-III-VI_2 crystals.

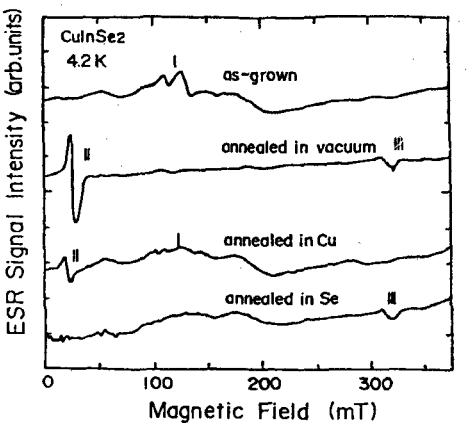

Fig. 4 Variation of ESR spectra by annealing in different atmosphere.

Acknowledgments

This work was supported in part by the New Energy and Industrial Technology Development Organization under the New Sunshine Project. The author expresses his sincere thanks to Dr. I. Aksenov for his contribution to this study.

REFERENCES

1. *Copper Indium Diselenides for Photovoltaic Applications*, eds. T.J. Coutts, L.L. Kazmerski and S. Wagner (Elsevier, Amsterdam, 1986)
2. I. Aksenov, N. Nishikawa and K. Sato, J. Appl. Phys. 74 (1993) 3811.
3. I. Aksenov and K. Sato, Jpn. J. Appl. Phys. 31 (1992) 2352.
4. K. Sato, I. Aksenov, N. Nishikawa and T. Kai, Jpn. J. Appl. Phys. 32 Suppl. 32-3 (1993) 481.
5. I. Aksenov, T. Kai, N. Nishikawa and K. Sato, Jpn. J. Appl. Phys. 32 (1993) 3391.
6. K. Sato and I. Aksenov, J. Cryst. Res. & Technol. (in press)
7. N. Nishikawa, I. Aksenov, T. Shinzato, T. Sakamoto and K. Sato, Jpn. J. Appl. Phys. 34 (1995) L975.
8. K. Sato, N. Nishikawa, I. Aksenov, T. Shinzato and H. Nakanishi, Jpn. J. Appl. Phys. 35 (1996) 2061.
9. W.G. Spitzer and J.M. Whelan, Phys. Rev. 114 (1959) 59.
10. G. Brandt, A. Räuber and J. Schneider, Solid State Commun. 12 (1973) 481.
11. W.C. Holton, M. DeWit, T.L. Estle, B. Dicher and J. Schneider, Phys. Rev. 169 (1968) 359.
12. J.M. Tchapkui-Niat, A. Goltzene and C. Schwab, J. Phys. C: Solid State Phys. 15 (1982) 4671.